Monthly Notices
of the
ROYAL ASTRONOMICAL SOCIETY

MNRAS **488,** 381–386 (2019)
Advance Access publication 2019 June 25

doi:10.1093/mnras/stz1735

Rotational quenching of HD induced by collisions with H_2 molecules

Yier Wan [1]★ N. Balakrishnan,[2] B. H. Yang,[1] R. C. Forrey[3] and P. C. Stancil[1]★

[1]*Department of Physics and Astronomy, Center for Simulational Physics, The University of Georgia, Athens, GA 30602, USA*
[2]*Department of Chemistry, University of Nevada, Las Vegas, NV 89154, USA*
[3]*Department of Physics, Penn State University, Berks Campus, Reading, PA 19610, USA*

Accepted 2019 June 12. Received 2019 June 7; in original form 2019 April 10

ABSTRACT

Rate coefficients for rotational transitions in HD induced by H_2 impact for rotational levels of HD $j \leq 8$ and temperatures 10 K $\leq T \leq$ 5000 K are reported. The quantum mechanical close-coupling (CC) method and the coupled-states (CS) decoupling approximation are used to obtain the cross-sections employing the most recent highly accurate H_2–H_2 potential energy surface (PES). Our results are in good agreement with previous calculations for low-lying rotational transitions The cooling efficiency of HD compared with H_2 and astrophysical applications are briefly discussed.

Key words: molecular data – molecular processes – scattering.

1 INTRODUCTION

Collisions involving H_2 and HD molecules are of crucial importance in early Universe chemistry (Puy et al. 1993; Galli & Palla 1998, 2002; Stancil, Lepp & Dalgarno 1998; Glover & Abel 2008), star formation (Ripamonti 2007; McGreer & Bryan 2008; Hirano et al. 2015), and the interstellar medium (ISM) environment (Lacour et al. 2005; Liszt 2015). While H_2 emission is difficult to detect, the far-infrared line emission of HD has been observed by a variety of facilities. The fundamental HD $j = 1 \rightarrow 0$ rotational line has been previously detected by the Infrared Space Observatory (ISO) Long Wavelength Spectrometer towards the Orion Bar (Wright et al. 1999) and the giant molecular cloud Sagittarius B2 (Polehampton et al. 2002); by *Herschel* Space Observatory in the TW Hya protoplanetary disc (PPD) (Bergin et al. 2013) and the Orion Bar (Joblin et al. 2018). Other transitions have also been detected towards the Orion molecular outflow by ISO (Wright et al. 1999); in supernova remnants and star-forming regions by the *Spitzer* Space Telescope (Neufeld et al. 2006). Finally, the HD $j = 4 \rightarrow 3$ line was predicted by Kamaya & Silk (2003) to be detectable by the Atacama Large Millimetre Array (ALMA) in proposed observations of primordial molecular clouds.

Although the abundance ratio of HD/H_2 is $\sim 10^{-3}$ in the early Universe (Stancil et al. 1998; Flower 2000, 2007), HD may contribute significantly relative to H_2 in cooling primordial gas. Unlike H_2, for which only quadrupole transitions are possible, HD has a small but finite dipole moment. Thus, $\Delta j = \pm 1$ transitions are allowed and spontaneous transition probabilities are much larger than the quadrupole transition probabilities in H_2. Besides, the small energy spacing of HD allows for enhanced excited state populations. The HD cooling rate can equal or surpass that of H_2 especially at low temperatures and cools the environment further down below 100 K.

Apart from being a coolant of astrophysical media, recent studies (Bergin et al. 2013; Favre et al. 2013; McClure et al. 2016; Trapman et al. 2017) have revealed that HD could serve as the tracer of PPD mass. Previously, a variety of diagnostics have been used to estimate the disc gas mass including dust thermal emission and CO rotational lines for PPDs. To infer the total mass from dust, knowledge of the local gas-to-dust ratio is needed, while CO rotational emission probes the surface of the outer disc inwards to the position of Mars. CO and water rovibrational lines originate in the inner disc. While the dominant constituent of the disk is H_2, its emission is limited to the warm inner disck(Kamp et al. 2018). As a consequence, disparate results are obtained from utilizing these emission features to estimate the disc gas mass. However, HD rotational emission probes a much larger fraction of the disc reaching from the surface down to the mid-plane. The utility of HD as a mass diagnostic was first pointed out by Bergin et al. (2013) who observed the HD $j = 1 \rightarrow 0$ rotational line in the disk of TW Hya with the *Herschel* PACS detector. Using PACS to observe six PPDs, McClure et al. (2016) detected the HD 112 μm line in DM Tau and GM Aur. They find that the disk masses deduced from prior CO observations are significantly smaller or at the lower end of their HD-derived masses.

In astrophysical environments having low molecular densities or experiencing a significant amount of external energy input, like shocks and UV radiation, molecular level populations will be driven out of equilibrium. It is necessary to solve a master equation to determine the level populations, which requires accurate molecular data for both radiative and collisional processes (Roueff & Lique 2013). In the early Universe, the most abundant collisional partners are H and He. We show below that the rates of HD in collision with H_2 are larger than those with H and He. The current available HD–H_2 collisional rate coefficients are limited to low temperatures and low-lying HD rotational levels. The lack of homonuclear symmetry

★ E-mail: yier.wan@uga.edu (YW); stancil@physast.uga.edu (PCS)

renders the cross-section calculations for HD more computationally expensive than for H_2, where the ortho- and para-H_2 states can be treated separately.

Initial studies of HD + H_2 collisions started with the work of Chu (1975). Later, Schaefer (1990) calculated rate coefficients for the excitation of HD by H_2, but only for the low-lying rotational levels ($j \leq 2$) and over a limited temperature range 10 K $\leq T \leq$ 300 K. Schaefer used the empirical isotropic potential fit of Farrar & Lee (1972), which includes only the A_{000} and A_{101} term of the HD–H_2 potential (see equation 1). Deficiencies of the interaction potential and especially of the anisotropic terms are usually the main source of errors of rotationally inelastic cross-sections and rate coefficients. Subsequently, Flower (1999) and Flower & Roueff (1999), who used the ab initio potential energy surface (PES) developed by Schwenke (1988), presented rate coefficients for kinetic temperatures $T \leq$ 1000 K and rotational levels of the HD molecule $j \leq 8$. Their results are comparable with those of Schaefer (1990) but significant differences were seen at relatively low temperatures. Sultanov & Guster (2007) and Sultanov, Khugaev & Guster (2009) have reported extensive calculations of rotational transitions in HD + H_2 collisions using a rigid rotor model and the six-dimensional PES of Boothroyd et al. (1991), referred to as the BMKP PES hereafter. Their studies yielded results in reasonable agreement with those of Schaefer (1990) for the dominant $\Delta j_1 = \pm 1$ transitions in HD with $j_1 \leq 2$ and $j_2 = 0, 1, 2$ (The rotational levels of HD and its collisional partner are denoted by j_1 and j_2 hereafter), but substantial differences were observed for $\Delta j_1 = \pm 2$ transitions in HD and transitions that involve exchange of two rotational quanta, such as (1,2) HD($j_1 = 1$) + $H_2(j_2 = 2) \rightarrow$ HD($j_1 = 2$) + $H_2(j_2 = 0)$. The more recent work of Sultanov, Guster & Adhikari (2012) using the four-dimensional PES of Diep & Johnson (2000), referred to as the DJ PES hereafter, and Sultanov, Guster & Adhikari (2015) which adopted the six-dimensional PES of Hinde (2008), appeared to be very different from previous studies. Balakrishnan et al. (2018) pointed out the inconsistency might question the validity of Schaefer's results which are generally considered to be accurate for rotational transitions in HD + H_2 collisions. They reproduced Schaefer's results quantitatively for most low-lying rotational transitions with two sets of calculations: (i) full-dimensional quantum close-coupling (CC) calculations using the Hinde PES and (ii) calculations within the rigid rotor model and using the four-dimensional PES developed by Patkowski et al. (2008), referred to as Patkowski PES hereafter. The excellent agreement in the two sets of calculations demonstrated that the four-dimensional rigid-rotor model is adequate to compute rotational transitions within the vibrational ground state of HD. The work of Balakrishnan et al. (2018) yielded almost identical result as that of Schaefer (1990), however, quite different from the work of Sultanov et al. Because both Sultanov et al. (2015) and Balakrishnan et al. (2018) employed the same Hinde PES and MOLSCAT (Hutson & Green 1994) scattering code, it is likely that the source of the discrepancy is some numerical error in the calculations of Sultanov et al., presumably arising from the coordinate transformation.

In this paper, we extend the work of Balakrishnan et al. (2018), to perform calculations of HD + H_2 collisions using the rigid rotor model and the Patkowski PES. New rate coefficients for rotational levels $j_1 \leq 8$ of the HD molecule over a wider temperature range, 10 K $\leq T \leq$ 5000 K are presented and compared with the work of Flower (1999). It is found that the results of Flower (1999) overestimated the rate coefficients at moderate temperatures, although they showed the right increasing trend in each transition. We also report critical densities of HD based on the HD + H_2 rate coefficients computed here. The paper is organized as follows. In Section 2 a brief description of the coordinate rotation to obtain the HD–H_2 PES from the H_2–H_2 PES as well as scattering calculations are given. The computed results are presented and compared with previous calculations in Section 3. Astrophysical applications of the rate coefficients are briefly discussed in 4, including the cooling efficiency and critical density. Finally, a summary of our results is given in Section 5. The transition HD(j_1) + X(j_2) $\rightarrow$ HD(j_1') + X(j_2) is denoted by $j_1 \rightarrow j_1'$ hereafter.

2 CALCULATION DETAILS

The PESs developed for the H_2–H_2 system can also be applied to the HD + H_2 collisions. Under the Born–Oppenheimer approximation, the H_2–HD interaction potential is identical to that of H_2–H_2. The main difference between H_2–H_2 and HD–H_2 is that the centre-of-mass of one of the H_2 molecules is displayed from the middle of the interatomic distance to the centre-of-mass of the HD molecule. A coordinate rotation that shifts the centre-of-mass of H_2 to HD similar to that adopted by Sultanov et al. (2012) is utilized to obtain the H_2–HD PES from the H_2–H_2 Patkowski PES. We followed the corrected coordinate rotation approach as described in the appendix of Balakrishnan et al. (2018).

Computations were carried out using the quantum CC method with a mixed-mode OpenMP/MPI version of the non-reactive scattering code MOLSCAT (Hutson & Green 1994) modified by Valiron & McBane (2008) and Walker (2013), referred to as VRRMM hereafter. Both the HD and H_2 molecules are treated as rigid rotors. The full quantum CC formulation is well documented in Green (1975). In the scattering calculations, the angular dependence of the interaction PES is expanded as

$$V(R, \theta_1, \theta_2, \phi) = \sum_{\lambda_1, \lambda_2, \lambda} A_{\lambda_1, \lambda_2, \lambda}(R) Y_{\lambda_1, \lambda_2, \lambda}(\theta_1, \theta_2, \phi), \quad (1)$$

where $A_{\lambda_1,\lambda_2,\lambda}(R)$ are radial expansion coefficients and $Y_{\lambda_1,\lambda_2,\lambda}(\theta_1, \theta_2, \phi)$ are the bispherical harmonics. (14, 14, 8) quadrature points are used for integration along each of the angular coordinates $(\theta_1, \theta_2, \phi)$. As discussed in Balakrishnan et al. (2018), the leading anisotropic terms on the HD–H_2 potential, A_{101} and A_{022}, are nearly identical for both the Hinde PES and Patkowski PES. We excluded any terms beyond A_{448}, because higher order terms do not make significant contributions and are not included in the PES of Patkowski et al. (2008).

The modified log-derivative Airy propagator of Alexander & Manolopoulos (1987) is applied to integrate the coupled channel equations and the log-derivative matrix propagated to sufficiently large intermolecular separations to yield converged results. The interval from $R = 1\ a_0$ to the asymptotic matching radius $R = 60\ a_0$ with a step size 0.05 a_0 is found to be adequate for the propagation. We also performed several convergence tests to verify the reliability of the computed collision data. Basis sets with [$0 \sim j_1 + 5$; $j_2 \sim j_2 + 4$] were found to be sufficiently large for collision energies smaller than 20 000 cm^{-1}. Basis sets [$0 \sim j_1 + 2$; $j_2 \sim j_2 + 4$] are sufficiently large for collision energies smaller than 1000 cm^{-1}.

Since the full CC calculation is prohibitively expensive at high collision energies, the coupled-state (CS) decoupling approximation (Heil, Green & Kouri 1978) is used for calculations for collision energies larger than 2000 cm^{-1}. The total wave function is expanded in the basis ϕ_{jl}^{JM} in the CC formulation, while in the CS formulation, $\phi_{j\Omega}^{JM}$ is chosen to be the basis sets, where j is the compact notation for quantum number set (j_1, j_2, j_{12}), l is the orbital angular momentum, J is the total angular momentum, M is its projection on a space-fixed axis, and Ω refers to the body-fixed projection of j_{12}. Due to the

Table 1. Cross-sections (10^{-16} cm^2) of HD($j_1 = 7$) + ortho-H_2($j_2 = 1$) collision calculated with CC method and CS approximation at a collision energy of 2000 cm^{-1}.

$j_1 \rightarrow j_1'$	CC[a]	CS[b]	per cent diff[c]
$7 \rightarrow 6$	2.0465	1.9845	3.0
$7 \rightarrow 5$	3.1159×10^{-1}	2.9848×10^{-1}	4.2
$7 \rightarrow 4$	5.9364×10^{-2}	5.5020×10^{-2}	7.3
$7 \rightarrow 3$	1.2419×10^{-2}	1.1299×10^{-2}	9.0
$7 \rightarrow 2$	2.5027×10^{-3}	2.2676×10^{-3}	9.4
$7 \rightarrow 1$	4.8284×10^{-4}	4.4082×10^{-4}	8.7
$7 \rightarrow 0$	6.9476×10^{-5}	6.4852×10^{-5}	6.7

[a]basis set [0 − 9; 1 − 5]
[b]basis set [0 − 12; 1 − 5]
[c]per cent diff $= |\sigma^{cs} - \sigma^{cc}|/\sigma^{cc}$

decoupling of l, the potential matrix in the CS approximation can be split into smaller sub-matrix blocks that in CC formulation, so the CS decoupling approximation is computationally cheaper. Table 1 presents a comparison of cross-sections for ortho-H_2 collisions using the full CC method and the CS approximation at high collision energies. The discrepancies between the two methods are small at high collision energies. Since a large number of partial waves are needed to obtain converged cross-sections for higher collision energies, utilizing the CS approximation is necessary to make the calculations feasible at high energy end. Similar results were obtained for para-H_2 collisions.

De-excitation rate coefficients were obtained by thermally averaging the cross-sections over a Boltzmann distribution of collision energies,

$$k_{j_1 j_2 \rightarrow j_1' j_2'}(T) = A \times \int_0^\infty \sigma_{j_1 j_2 \rightarrow j_1' j_2'}(E_k) e^{(-E_k/k_B T)} E_k \, dE_k, \qquad (2)$$

where $A = \frac{1}{(k_B T)^2} \left(\frac{8 k_B T}{\pi \mu}\right)^{1/2}$, E_k is the kinetic energy, k_B is the Boltzmann constant, μ is the reduced mass of the collision system, and $\sigma_{j_1 j_2 \rightarrow j_1' j_2'}(E_k)$ is the state-to-state cross-section.

3 RESULTS AND DISCUSSION

First, a comparison of cross-sections calculated using the Patkowski and Hinde PESs is presented in Fig. 1. It is seen that both calculations yield essentially identical results when the relative velocity is larger than 200 m s^{-1} and the results are in agreement with previous work of Schaefer (1990). In both cases, the rigid rotor approximation and the same quantum scattering code MOLSCAT/VRRMM is adopted, so that the discrepancies mainly come from the minor differences in the PESs. Whereas the discrepancies in the resonant region and at lower velocities are attributed to the increased sensitivity of cross-sections to fine details of the PES, they are not significant at astrophysically relevant temperatures.

Rate coefficients for the $j_1 = 2 \rightarrow j_1' = 1, 0$ transitions are presented in Fig. 2. The differences between the cross-sections at low collision energies manifest in the rate coefficients at temperatures below 10 K. It is seen that the present results on the Hinde and Patkowski PESs agree with that of Schaefer (1990). The results of Flower (1999) are somewhat larger for the $j_1 = 2 \rightarrow j_1' = 1$ transition, but in good agreement for the $j_1 = 2 \rightarrow j_1' = 0$ case. The rate coefficient for HD in collision with He and H are also plotted in Fig. 2 for comparison. As one can see, both the HD–H and HD–He rate coefficients are smaller than the rates of HD + H_2 collisions. For the $j_1 = 2 \rightarrow 0$ transition in collision with ortho-H_2, the rate coefficients of HD is larger by a factor of ∼5 than that of H_2.

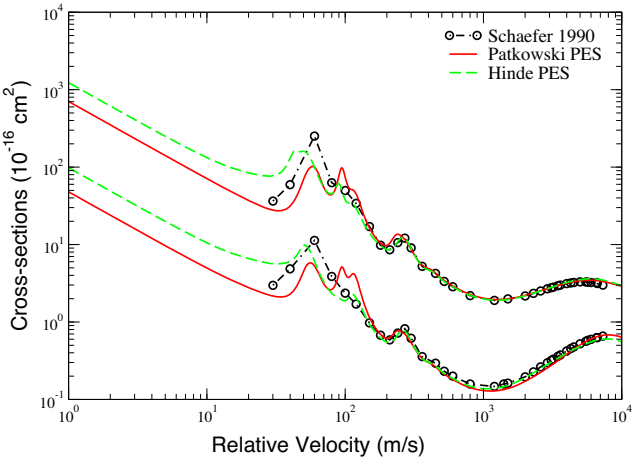

Figure 1. Cross-sections for $j_1 = 2 \rightarrow 1, 0$ transitions in HD induced by collisions with ground-state ortho-H_2. The red solid curves as well as the green dash curves are calculations from this work. The black circles denote the work of Schaefer (1990).

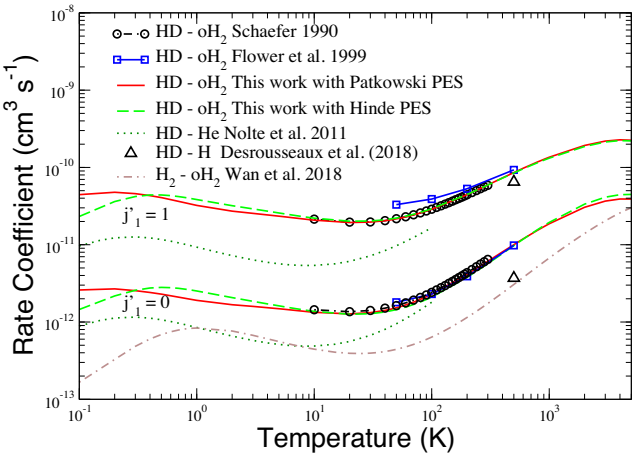

Figure 2. Rate coefficients for the $j_1 = 2 \rightarrow j_1' = 1, 0$ transitions in HD induced by different colliders. The red solid curves as well as the green dash curves are calculations from this work. The black circles denote the results of Schaefer (1990). Blue squares denote the work of Flower (1999). The HD–He, HD–H, and H_2–H_2 calculations are from Nolte et al. (2011), Desrousseaux et al. (2018), and Wan et al. (2018), respectively.

Fig. 3 shows cross-sections for $\Delta j_1 = -1$ transitions in HD + para-H_2 collisions. Transition $j_1 = 1 \rightarrow 0$ has two prominent resonances at about 10^{-5} and 4×10^{-4} eV. The latter resonance feature also appears in other quenching transitions at the same position with similar width from higher initial states, while the complexity of the 10^{-5} eV resonance feature increases as j_1 increases. Whereas previous analysis have revealed that the positions of low-energy resonances depend sensitively on the PES, this has little effect on the reliability of quenching rates at temperatures of astrophysical interest (10 K $\leq T \leq$ 5000 K). Fig. 4 presents cross-sections for $\Delta j_1 = -1$ transitions in HD + ortho-H_2 collisions. Similar to Fig. 3, there is a prominent resonance appearing at about 4×10^{-4} eV and additional resonances appearing at lower collision energies. The very low energy behaviour of $j_1 = 1 \rightarrow 0$ indicates a zero-energy resonance corresponding to s-wave scattering in the

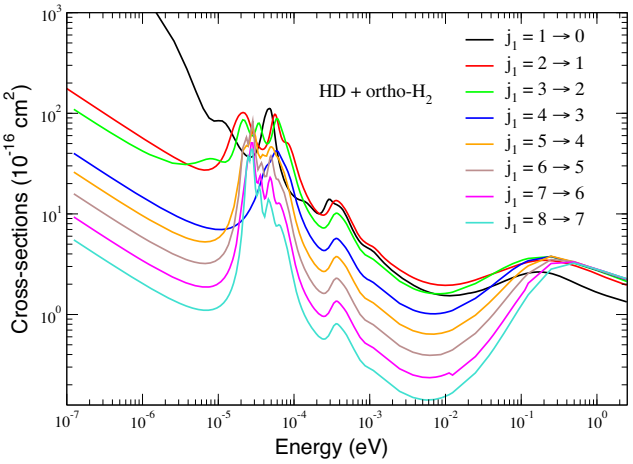

Figure 3. Cross-sections for the $\Delta j_1 = -1$ transitions of HD induced by ground-state para-H_2 as functions of the collision energy.

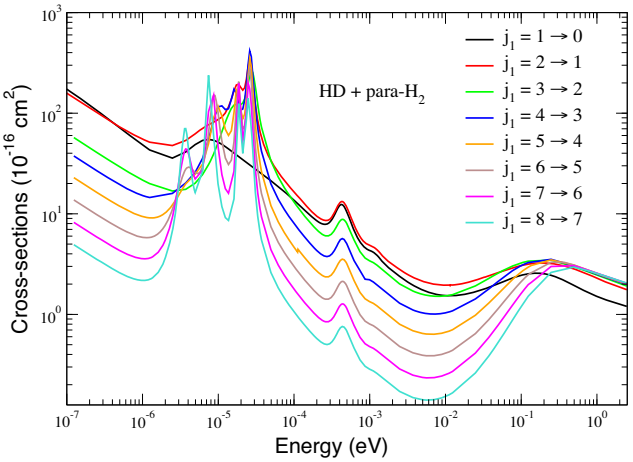

Figure 4. Cross-sections for the $\Delta j_1 = -1$ transitions of HD induced by ground-state ortho-H_2 as functions of the collision energy.

incident channel. In both figures, the cross-sections for quenching transitions from rotational levels $j_1 = 2$, 3 of HD are comparable with the quenching transition from $j_1 = 1$. At high collision energies (above 0.1 eV), $\Delta j_1 = -1$ transitions from rotational levels $j_1 = 2$–8 of HD have higher cross-sections than the $j_1 = 1 \rightarrow 0$ transition.

Fig. 5 displays the corresponding rate coefficients for the $\Delta j_1 = -1$ transitions in HD + para-H_2 collisions. It is seen that the $j_1 = 1 \rightarrow 0$ and $j_1 = 2 \rightarrow 1$ transitions are nearly identical with the available results of Schaefer (1990). While rate coefficients of the $j_1 = 6 \rightarrow 5$ transition display good agreement with that of Flower (1999), for other $\Delta j_1 = -1$ transitions with initial rotational levels $j_1 = 1$–5, Flower's results are generally larger values below 200 K. This is most likely due to the different treatment of the PES, especially the uncertainties in the higher order angular anisotropic terms employed in the earlier calculations. Fig. 6 shows rate coefficients of the $\Delta j_1 = -1$ transitions in HD + ortho-H_2 collisions. Similarly, good agreement is found with the work of Schaefer (1990). Noticeable differences between the present calculations and the work of Flower (1999) are observed for the low-lying transitions, while consistency in global trends improves with increasing temperature. Flower's results and this work show very good agreement, for the $6 \rightarrow 5$, $7 \rightarrow 6$, and $8 \rightarrow 7$ transitions.

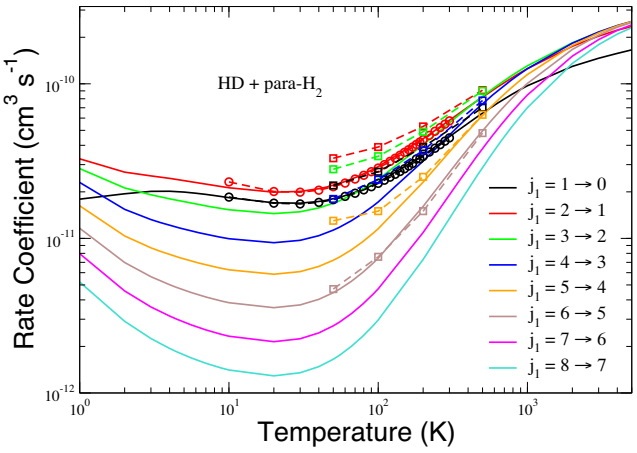

Figure 5. Temperature dependence of rotational state-resolved rate coefficients for transitions of HD induced by ground-state para-H_2. Solid curves represent calculations from this work. Squares denote the work of Flower (1999), while circles denote the results from Schaefer (1990).

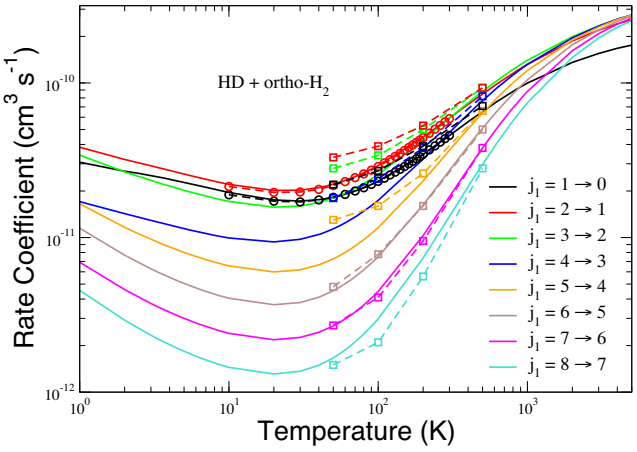

Figure 6. Temperature dependence of rotational state-resolved rate coefficients for transitions of HD induced by ground-state ortho-H_2. Solid curves represent calculations from this work. Squares denote the work of Flower (1999), while circles denote the results from Schaefer (1990).

4 ASTROPHYSICAL APPLICATIONS

Whereas the HD/H_2 abundance ratio is significantly smaller than 1, the contribution of HD in the thermal balance may become comparable to H_2 and even more important in certain circumstances, such as the cooling of primordial gas at high densities or low temperatures. During primordial star formation in low-mass haloes, the HD cooling rate can equal or surpass that of H_2, lowering the environment temperature below 100 K (Galli & Palla 2002; Lipovka, Núnez-López & Avila-Reese 2005).

We computed the cooling efficiency for HD and H_2 in collisions with the ground-state para-H_2. The low-density limit cooling rate is given by

$$\Lambda_{\rm HD} = n_{\rm HD} W_{\rm HD}, \tag{3}$$

where $n_{\rm HD}$ is the HD number density and $W_{\rm HD}$ is the HD cooling function in unit of erg s^{-1}. The cooling function is calculated by

$$W_{\rm HD}(T) = n(j_2) k_{j_1' j_2 \rightarrow j_1 j_2} h\nu_{j_1' j_1}, \tag{4}$$

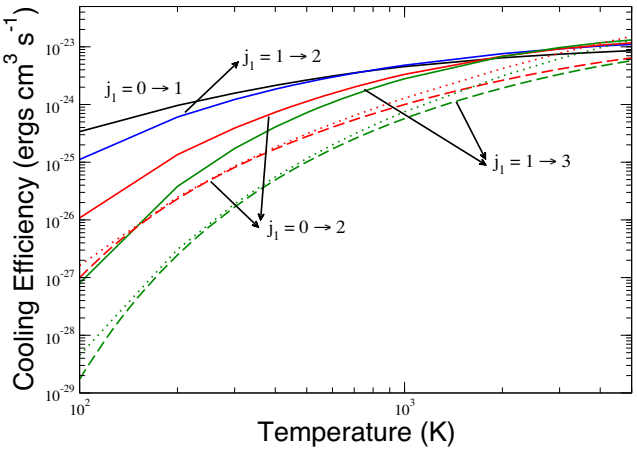

Figure 7. Cooling efficiency, $W_x/n(j_2)$, for HD and H_2 in collisions with ground-state para-H_2 for the indicated transitions. The solid curves denote HD cooling. The dashed curves denote H_2 cooling, based on the H_2–H_2 rate coefficients of Wan et al. (2018) and the dot curves denote the H_2 cooling fit of Glover & Abel (2008).

where $n(j_2)$ is the number density of the collision partner in collisions with HD, $h\nu_{j_1' j_1}$ is the emitted photon energy, and the excitation rate coefficient $k_{j_1' j_2 \rightarrow j_1 j_2}(T)$ can be obtained from quenching rates using detailed balance,

$$k_{j_1' j_2 \rightarrow j_1 j_2}(T) = \frac{w_{j_1}}{w_{j_1'}} k_{j_1 j_2 \rightarrow j_1' j_2}(T) \exp(-h\nu_{j_1' j_1}/kT), \quad (5)$$

where w_{j_1} and $w_{j_1'}$ are statistical weights for the upper and lower levels, respectively.

The cooling efficiencies, $W_{\rm HD}/n(j_2)$, and $W_{\rm H_2}/n(j_2)$ are shown in Fig. 7. It is clear that the cooling efficiency of HD is much higher than that of H_2, which allows HD to cool gas to lower temperatures more efficiently than that could be reached with H_2 alone. This effect results primarily from the smaller rotational constant of HD and the fact that the $j_1 = 0 \rightarrow 1$ transition is allowed.

For environments experiencing a significant departure from local thermodynamic equilibrium (LTE), the accurate calculations of the state-to-state rate coefficients are essential for a proper determination of the level populations. A non-LTE analysis is required, when the density of the molecule is smaller than the critical density for a given state j_1. The critical density for each rotational level j_1 can be written as (Osterbrock & Ferland 2006)

$$n_c(j_1) = \frac{\sum_{j_1' < j_1} A_{j_1 \rightarrow j_1'}}{\sum_{j_1' \neq j_1} k_{j_1 \rightarrow j_1'}}, \quad (6)$$

where $A_{j_1 \rightarrow j_1'}$ is the spontaneous transition probability.

In Fig. 8, we give the critical densities for HD. They are comparable for transitions induced by para- and ortho-H_2. Fig. 9 presents a comparison of critical densities in HD + para-H_2 and H_2 + para-H_2 collisions. Generally, HD requires larger gas densities to establish LTE than H_2, except for $j_1 > 6$ and temperatures less than ∼100 K.

5 SUMMARY

We performed extensive quantum mechanical coupled channel calculations for HD–H_2 collisions based on an accurate four-dimensional H_2–H_2 PES by Patkowski et al. (2008). Quenching rate coefficients with initial rotational levels $j_1 = 1$–8 of HD and $j_2 = 0$, 1 of H_2 for temperatures ranging from 10 to 5000 K are presented.

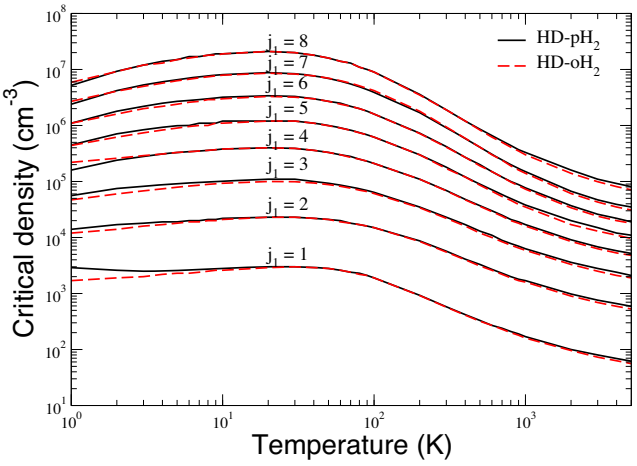

Figure 8. Critical densities for HD + para-H_2 (black solid curve) and HD + ortho-H_2 (red dash curve) as functions of gas temperature.

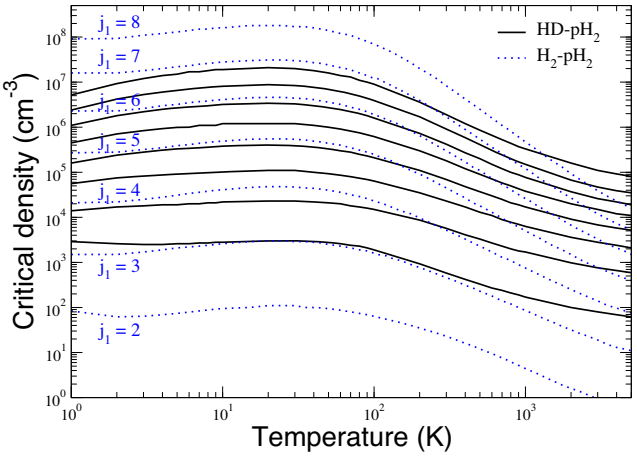

Figure 9. Critical densities for HD + para-H_2 (black solid curve) and H_2 + para-H_2 (blue dots) as functions of gas temperature. From bottom to top, each black curve represents rotational levels from j_1 =1 to 8 for HD molecule. The rotational level (j_1) of H_2 is labelled corresponding to each blue dash curve.

These data, derived using the most accurate PES for the H_2–H_2 system and a large basis set for the scattering calculation, should lead to more accurate rate coefficients for rotational transitions in HD + H_2 collisions for astrophysical modelling. The full data set is available online.[1]

ACKNOWLEDGEMENTS

This research used resources of the Georgia Advanced Computing Resource Center, the UNLV National Supercomputing Institute, and the Center for Simulational Physics of The University of Georgia. This work was funded by NASA HST Grant HST-AR-13899, NSF PHY-1806334 (NB), and NSF PHY-1806180 (RCF). We thank Konrad Patkowski for providing his H_2–H_2 PES.

[1]Rate coefficient data in the Leiden Atomic and Molecular Database (LAMDA; Schoier et al. 2005) format can be obtained at www.physast.uga.edu/amdbs/excitation/.

REFERENCES

Alexander M. H., Manolopoulos D. E., 1987, J. Chem. Phys., 86, 2044
Balakrishnan N., Croft J. F. E., Yang B. H., Forrey R. C., Stancil P. C., 2018, ApJ, 866, 95
Bergin E. A. et al., 2013, Nature, 493, 644
Boothroyd A. I., Dove J. E., Keogh W. J., Martin P. G., Peterson M. R., 1991, J. Chem. Phys., 95, 4331
Chu S. I., 1975, J. Chem. Phys., 62, 4089
Desrousseaux B., Coppola C. M., Kazandjian M. V., Lique F., 2018, J. Phys. Chem. A, 122, 8390
Diep P., Johnson J. K., 2000, J. Chem. Phys., 112, 4465
Farrar J. M., Lee Y. T., 1972, J. Chem. Phys., 57, 5492
Favre C., Cleeves L. I., Bergin E. A., Qi C., Blake G. A., 2013, ApJ, 776, L38
Flower D., 1999, J. Phys. B: At. Mol. Opt. Phys., 32, 1755
Flower D. R., 2000, MNRAS, 318, 875
Flower D. J., 2007, Molecular Collisions in the Interstellar Medium. Cambridge University Press, Cambridge, p. 36
Flower D. R., Roueff E., 1999, MNRAS, 309, 833
Galli D., Palla F., 1998, A&A, 335, 403
Galli D., Palla F., 2002, Planet. Space Sci., 50, 1197
Glover S. C. O., Abel T., 2008, MNRAS, 388, 1627
Green S., 1975, J. Chem. Phys., 62, 2271
Heil T. G., Kouri D. J., Green S., 1978, J. Chem. Phys., 68, 2562
Hinde R. J., 2008, J. Chem. Phys., 128, 154308
Hirano S., Hosokawa T., Yoshida N., Omukai K., Yorke H. W., 2015, MNRAS, 448, 568
Hutson J. M., Green S., 1994, MOLSCAT ver. 14 (distributed by Collaborative Computational Project 6; Daresbury Laboratory: UK Eng. Phys.Sci. Res. Council), http://www.giss.nasa.gov/tools/molscat/
Joblin C. et al., 2018, A&A, 615, A129
Kamaya H., Silk J., 2003, MNRAS, 339, 1256
Kamp I., Antonellini S., Carmona A., Ilee J., Rab C., 2017, The Cosmic Wheel and the Legacy of the AKARI archive: from galaxies and stars to planets and life, preprint (arXiv:1712.00303)
Lacour S. et al., 2005, A&A, 430, 967
Lipovka A., Núnez-López R., Avila-Reese V., 2005, MNRAS, 361, 850
Liszt H. S., 2015, ApJ, 799, 66
McClure M. K. et al., 2016, ApJ, 831, 167
McGreer I. D., Bryan G. L., 2008, ApJ, 685, 8
Neufeld D. A. et al., 2006, ApJ, 647, L33
Nolte J., Stancil P., Lee T.-G., Balakrishnan N., Forrey R., 2011, ApJ, 744, 62
Osterbrock D. E., Ferland G. J., 2006, Astrophysics of Gaseous Nebulae and Active Galactic Nuclei, 2 edn. Sausalito: Univ. Science, 2nd edn.. Univ. Science Books, Sausalito, CA
Patkowski K., Cencek W., Jankowski P., Szalewicz K., Mehl J. B., Garberoglio G., Harvey A. H., 2008, J. Chem. Phys., 129, 094304
Polehampton E. T., Baluteau J.-P., Ceccarelli C., Swinyard B. M., Caux E., 2002, A&A, 388, L44
Puy D., Alecian G., Le Bourlot J., Leorat J., Pineau Des Forets G., 1993, A&A, 267, 337
Ripamonti E., 2007, MNRAS, 376, 709
Roueff E., Lique F., 2013, Chem. Rev., 113, 8906
Schaefer J., 1990, A&AS, 85, 1101
Schöier F. L., van der Tak F. F. S., van Dishoeck E. F., Black J. H., 2005, A&A , 432, 369
Schwenke D. W., 1988, J. Chem. Phys., 89, 2076
Stancil P. C., Lepp S., Dalgarno A., 1998, ApJ, 509, 1
Sultanov R. A., Guster D., 2007, Chem. Phys. Lett., 436, 19
Sultanov R. A., Khugaev A. V., Guster D., 2009, Chem. Phys. Lett., 475, 175
Sultanov R. A., Guster D., Adhikari S. K., 2012, AIP Adv., 2, 012181
Sultanov R. A., Guster D., Adhikari S., 2015, J. Phys. B: At. Mol. Opt. Phys., 49, 015203
Trapman L., Miotello A., Kama M., van Dishoeck E. F., Bruderer S., 2017, A&A, 605, A69
Valiron P., McBane G. C., 2008, Mixed MPI and OpenMP extension ofthe MOLSCAT v14 package, http://ipag.osug.fr/ faurea/molscat/
Walker K. M., 2013, VRRMM (Vibrational/Rotational Rich Man's MOLSCAT), https://www.physast.uga.edu/research/stancil-group/protected/molecular
Wan Y., Yang B. H., Stancil P. C., Balakrishnan N., Parekh N. J., Forrey R. C., 2018, ApJ, 862, 132
Wright C. M., van Dishoeck E. F., Cox P., Sidher S. D., Kessler M. F., 1999, ApJ, 515, L29

SUPPORTING INFORMATION

Supplementary data are available at *MNRAS* online.

HDH2lamda_2019.dat

Please note: Oxford University Press is not responsible for the content or functionality of any supporting materials supplied by the authors. Any queries (other than missing material) should be directed to the corresponding author for the article.

This paper has been typeset from a TEX/LATEX file prepared by the author.